Kerr-gated time-resolved Raman spectroscopy of equine cortical bone tissue

Michael D. Morris
University of Michigan
Department of Chemistry
Ann Arbor, Michigan 48109
E-mail: mdmorris@umich.edu

Pavel Matousek
Michael Towrie
Anthony W. Parker
CCLRC Rutherford Appleton Laboratory
Central Laser Facility
Chilton, Didcot, Oxfordshire, OX11 0QX
United Kingdom

Allen E. Goodship
Edward R. C. Draper
Royal Veterinary College
Hawkshead Lane
North Mymms, Hatfield, Hertfordshire AL9 7TA
United Kingdom

Abstract. Picosecond time-resolved Raman spectroscopy in equine cortical bone tissue is demonstrated. Using 400-nm pulsed laser excitation (1 ps at 1 kHz) it is shown that Kerr cell gating with a 4-ps window provides simultaneously time-resolved rejection of fluorescence and time-resolved Raman scatter enabling depth profiling through tissue. The Raman shifts are the same as those observed by conventional cw Raman spectroscopy using deep-red or near-infrared lasers. The time decay of Raman photons is shown to fit an inverse square root of time function, suggesting propagation by a diffusive mechanism. Using polystyrene behind a bone specimen, it is shown that the 400-nm laser light penetrates at least 0.31 mm below the surface of a fully mineralized bone tissue specimen and generates observable bone Raman scatter (approximately 415 to 430 nm) through most of this depth. These novel results demonstrate great promise for *in vivo* applications for studying diseased bone tissue, and ways to optimize the setup are discussed. [DOI: 10.1117/1.1827605]

Keywords: Raman spectroscopy; photon migration; bone.

Paper 03116 received Sep. 19, 2003; revised manuscript received Apr. 1, 2004 and Jun. 10, 2004; accepted for publication Jun. 15, 2004; published online Jan. 31, 2005.

1 Introduction

Most tissue specimens exhibit intense fluorescence when excited with visible laser light and scatter light at all wavelengths at which Raman spectroscopy with silicon photodetectors is feasible. For these reasons workers in Raman tissue spectroscopy have generally employed near-infrared (NIR) lasers to obtain spectra from specimens. The most common sources have been diode lasers operating at 785 or 830 nm. While this approach is satisfactory in many cases, there are also disadvantages to long wavelength excitation.

For example, Raman scattering varies approximately with the inverse fourth power of exciting laser wavelength, so spectra are inherently only 1/5th or 1/6th as intense as spectra excited with green lasers, such as Nd:YAG 532 nm. Equally importantly, the quantum efficiency of silicon detectors falls off strongly above 900 nm, causing a further 2 to 3 times loss in signal, compared to green laser excitation. As a consequence, investigators resort to the use of high laser power, long integration times, or both.

In tissue, multiple scattering is a more important source of attenuation of light in the 400- to 1000-nm range than absorption, except for wavelengths at which hemoglobin, or in transcutaneous measurements hemoglobin and melanin, absorb strongly. Light propagation under these conditions is called photon migration in the biomedical optics literature and is a widely studied phenomenon. A recently published handbook[1] provides reviews of both theory and applications from several different perspectives. To a good first approximation, multiple scattering can be modeled as a random walk, analogous to diffusion. Photons that are detected after multiple scattering events are generally called diffusive photons. This scattering is the dominant phenomenon when using NIR radiation that is preferred for deep penetration into tissue.

However, while NIR wavelengths are advantageous for optimum penetration depth, to date most tissue studies using Raman spectroscopy have been performed by interrogation of only the outermost layers of specimens. Raman detection of dysplasia in epithelial tissues is perhaps the most widely studied example.[2–5] In a few cases, subsurface tissue has been probed. For example, Feld and co-workers have used Raman spectroscopy for measurement of cholesterol in blood vessels.[6] Puppels and co-workers have demonstrated 50-μm penetration in depth-resolved Raman measurement of water content of skin.[7] Both groups commented on the light scattering properties of their specimens.

Despite the extensive literature of time-resolved photon migration measurements in absorption and fluorescence spectroscopies, Raman photon migration has been studied only infrequently. The earliest studies demonstrated the phenomenon in turbid media such as suspensions of polystyrene spheres[8] and milk.[9]

Everall and co-workers have characterized Raman photon migration in finely divided powders that scatter light strongly.[10] Furthermore, for powdered samples of trans-

Address all correspondence to: Michael D. Morris, University of Michigan, Department of Chemistry, 930 N. University Ave., Ann Arbor, MI 48109-1055; Tel: 734-764-7360; Fax: 734-764-8815; E-mail: mdmorris@umich.edu

1083-3668/2005/$22.00 © 2005 SPIE

stilbene and poly(aryl-ether-ether-ketone) (PEEK) it was shown that Raman signals generated from 400-nm illumination are recovered from depths of several millimeters and that the total photon migration distance is at least 3 cm as determined by monitoring the delay between the 1-ps laser excitation pulse and temporally discriminating the late-arriving Raman photons.

This group presented the first detailed studies of the time evolution of Raman scatter generated by diffusive photons. They found the time decay of the Raman scattering intensity observed at a single point outside the powder to follow a $t^{-1/2}$ dependence and elastically scattered light followed a $t^{-3/2}$ decay where t is the time following the 1-ps excitation pulse. The time dependences of both Raman and Rayleigh scatter were explained by simple diffusion models and developed without reference to the biomedical photon migration literature. Thus, in more recent work the same group has presented Monte Carlo simulations of the decay of Raman and scatter under realistic boundary conditions for a laboratory optical system[11] and recognized the association of their work with photon migration studies.

It has been known for many years that fluorescence can be separated from Raman scatter by time-gating the signals.[12] Ideally, in optically transparent media, Eq. (1) applies:

$$f_{R/B}=\frac{1}{[1-e^{-\tau_g/\tau_f}]}. \tag{1}$$

In Eq. (1), $f_{R/B}$ is the improvement of the ratio of Raman scatter to background compared to dc measurement of the total signal, while τ_g and τ_f are the gate time and fluorescence lifetime respectively. Many important fluorophores have fluorescence lifetimes in the 1- to 5-ns range and therefore a gate width in the low picosecond range is needed for effective fluorescence suppression. For example, the fluorescence lifetime for tryptophan is about 3.1 ns.[13] Common gating techniques, such as those based on electrical switching, do not provide the necessary picosecond response time. For example, the fastest gated image intensifiers presently available provide 50-ps opening times and the most commonly available intensifiers operate with gate widths of a few nanoseconds.

It is only recently that the technology to exploit time-gated fluorescence rejection has been possible. Using a 1-kHz repetition rate laser system giving 1-ps pulse widths, Matousek and co-workers have demonstrated that a Kerr cell placed before the Raman spectrograph entrance slit functions as an ultrafast optical shutter with an ~4-ps opening time and provides a ratio of 10^5 between the open and closed state.[14] With a 1-ps laser generating the Raman spectrum they have obtained fluorescence rejection of up to 1000 times. The Kerr cell gate opening time relative to the Raman excitation pulse can be adjusted over a wide range using a variable distance optical delay line.[11] Further increases in rejection are available by such strategies as combination of time gating and shifted excitation difference measurements.[15] There has also been one early report of the use of a streak camera for time-resolved Raman spectroscopy.[16] A time-resolution of approximately 10 ps was achieved, but noise in the intensifier limited the quality of the spectrum. The streak camera does provide data from a range of time delays simultaneously, and this property could prove useful in depth resolution.

In this work we report further exploitation of the Kerr cell gating technology for time-gated and time-delayed Raman spectroscopy.

Bone tissue is a composite material containing a carbonated apatite mineral phase and an organic matrix phase that is about 90% type I collagen. The basic vibrational (Raman and infrared) spectroscopy of bone tissue has been reviewed.[17] Both methods of obtaining vibrational spectra provide similar information on the composition and local structure of both the mineral and matrix components. In general, Raman spectroscopy provides somewhat narrower bands, better spatial resolution, and the ability to probe both thin and thick specimens, while infrared spectroscopy provides generally higher signal/noise ratio but only for specimens a few micrometers thick. Infrared spectroscopy has the additional advantage of a longer history of empirical and theoretical band assignments for the bands of proteins.

In both Raman and infrared spectra of bone tissue the amide I (C=O stretch) and amide III (C-N stretch, C-H bend) bands contain a wealth of information. Both bands are envelopes that are resolvable into three or more components. The relative intensities of the bands in the amide I envelope vary with the number and type of interfibril cross-links and in normal mature tissue the most intense component is at 1665 cm^{-1}. In immature tissue[18] or in tissue in which the cross-links have been severed mechanically[19] or partially disrupted chemically, a band at 1685 to 1690 cm^{-1} is prominent.

In this communication we describe the first use of picosecond time-gated Raman spectroscopy on a tissue specimen. Blue (400-nm) excitation and a short gate interval are used because the laser system is part of a national user facility and is optimized for these conditions to maximize its utility to many investigators. The goal of this preliminary investigation is to demonstrate the potential benefits of using Kerr-gated Raman for analyzing tissue and that depth profiling below the surface is possible. Once this is demonstrated the next step will be to optimize both the excitation wavelength and the wavelength to drive the Kerr gate. Operation in the Soret band of heme simultaneously demonstrates fluorescence rejection, the potential for resonance enhancement, and the potential for depth-resolved Raman photon migration measurements in bone tissue specimens. In addition to its continuing interest to the authors, bone tissue has the advantage for exploratory studies in spectroscopic technology that the Raman bands of the mineral component are easily distinguished from the Raman bands of surrounding soft tissues.

2 Experiment

2.1 *Instrumentation*

The Kerr-gated picosecond Raman spectroscopy system has been described in detail elsewhere.[20] An argon ion laser is used to pump a femtosecond mode-locked Ti:sapphire laser, which is amplified by an Nd:YLF-pumped regenerative amplifier to generate 1-ps pulses at 800 nm. A beam splitter isolates a 500-μJ pulse from this laser to drive the Kerr cell, while the remainder of the pulse is frequency-doubled. The 400-nm pulse is used to drive an optical parametric amplifier,

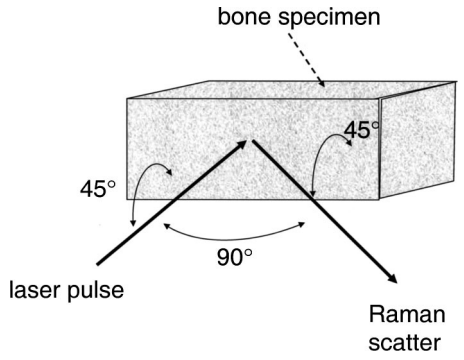

Fig. 1 Bone tissue specimen illumination/collection geometry. The specimen is oriented at 45 deg with respect to the incident laser beam.

allowing generation of tunable laser light at any desired wavelength in the 470- to 700-nm range, or is directly used in experiments as a probe. An optical delay line allows sequencing of the pulses with an accuracy of 50 fs across a time range of 6 ns. Delays of 0 to 50 ps were used in this work. Experiments were performed at 400 nm using the second harmonic of the fundamental regenerative amplifier output. At this wavelength the pulse energy at the specimen was 8 μJ and the average power was 8 mW.

The Raman spectrograph and illumination/collection optics are conventional. The specimen illumination/Raman scatter collection geometry is shown in Fig. 1. Laser light was focused onto the specimen at an angle of 45 deg using a 50-cm focal length lens to produce a spot size of 0.2 mm. Scattered light was collected from the incident face of the sample at 90 deg with respect to the probe pulse direction (at 45 deg respective to the sample plane) using a 25-mm focal length f/0.85 video lens (Fujinon) and passed through the Kerr gate optics to a single stage 0.5-m spectrograph (Spex) fitted with a 1200-grooves/mm grating with an entrance slit width set to give 15 cm^{-1} resolution. The dispersed light was detected by a cryogenically-cooled 2000×800-pixel back-thinned CCD (ISA) with a horizontal pixel binning parameter set to 5. Again, the 400-nm Raman source was used as optimum for the collection and detection system. The emphasis of this study is to prove the feasibility of applying the Kerr gate to tissue samples in general. The detector output was stored on a personal computer that also controls all other instrument parameters. The spectrograph wavenumber scale was calibrated against acetonitrile. The instrument was checked for drift periodically using the Raman spectrum generated from a piece of Teflon (polytetrafluoroethylene) or other commercially available polymers as a secondary standard. All data reduction was performed in GRAMS/AI (ThermoGalactic). Background was removed by subtracting a cubic polynomial obtained by fitting 8 to 10 points in the spectrum. Peak positions and intensities were calculated using the built-in GRAMS functions. Except as noted in the text, displayed spectra have been background-corrected. No smoothing or low pass filtering has been applied to the spectra.

Raman spectra from each bone specimen were collected from three different locations separated by several millimeters. Two Raman spectra were collected from each of the locations to verify spectra reproducibility.

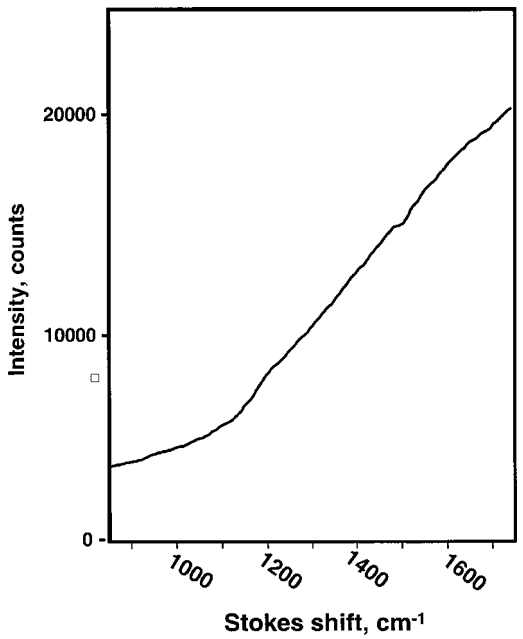

Fig. 2 Ungated spectrum of equine cortical bone tissue obtained using 400-nm excitation. Laser: 400 nm, 8 mW focused to 200-μm diameter spot. Total exposure time 320 s. Note: No Raman features are recoverable from the spectrum (see text).

Measurement of the depth of penetration through bone specimens and measurement of photon diffusion properties were performed on specimens ground to about 0.22 mm and mounted at a 45-deg angle to the incident laser beam as described above to give an effective depth of 0.31 mm. The time dependence of the signals was found by delaying the opening of the Kerr gate from 0 to 30 ps in 4- to 10-ps increments relative to the incident 1-ps Raman excitation pulse. A small sample of powdered polystyrene placed against the back of the specimen was used to identify Raman scatter arising from beyond the depth of the specimen. The time dependence of the laser light scattering from the sample was used to further characterize the depth of penetration.

2.2 *Materials*

Standard beam samples (10-mm wide, 5-mm deep, and 45-mm long) were cut under constant irrigation from the proximal, dorsal cortex of the third metacarpal (canon) bone. These bones were collected from local registered abattoirs from skeletally mature horses and frozen within 24 hours of death and thawed immediately before tissue preparation or testing. Each sample was thawed and refrozen three times, first to cut the bone beams, second for mechanical testing, and finally for spectroscopic analysis. All the bone samples were double wrapped (the cut was also covered in gauze soaked in 0.9% saline) before freezing to prevent dehydration.

3 Results and Discussion

Figure 2 shows the uncorrected spectrum of a bone specimen obtained with the Kerr gate open through the entire data collection period. There is no time resolution in this experiment. Although the laser outputs a train of picosecond pulses, in the ungated mode the instrument is operating as a pseudo-cw Ra-

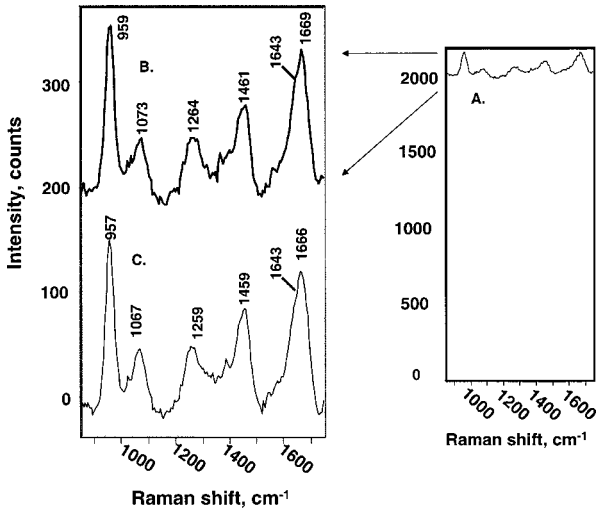

Fig. 3 Two replicate (consecutive) measurements of the Kerr-gated Raman spectrum of a specimen of equine cortical bone tissue. The 4-ps gate is adjusted for maximum signal (zero delay). Exposure conditions: 400 nm, 8 mW focused to 200-μm diameter spot; 400 s total laser exposure time. For discussion of the bands, see text and Table 1. A. The Raman spectrum as collected, without background subtraction. B. The spectrum of trace A after background subtraction. C. Another spectrum obtained at the same location on specimen as trace A. The spectra are offset for clarity.

man spectrograph. As can be seen, the signal in Fig. 2 is dominated by fluorescence. We noted that in the first second of sample irradiation the background was even higher and this is believed to be to an unidentified fluorophore in the bone that was quickly photobleached. No further photochemical decay was observed as evidenced by no changes in Raman signals during data acquisition.

We were not able to recover any Raman bands above the ungated fluorescence background even after extensive data processing. The only features found on the otherwise smooth spectrum are attributable to the wavelength dependences of detector quantum efficiency and grating diffraction efficiency. Numerous chromophores present in bone tissue including collagen and hemoglobin fluoresce when excited at 400 nm and any or all of them could contribute to the emission. As is generally true for tissue specimens, cw laser excitation at this deep blue (400-nm) wavelength is not suitable for bone tissue Raman spectroscopy.

Figure 3 shows Kerr-gated Raman spectra of a specimen of horse cortical bone. A 4-ps Kerr gate is used with zero delay time between gate opening and the excitation pulse. That is, the delay line was positioned to maximize the Raman spectrum seen at the detector. Trace A shows the spectrum as recorded. Trace B shows the same spectrum at larger scale after removal of background. Traces B and C show the spectra taken sequentially at exactly the same place on the specimen. The spectra are offset for clarity.

Assuming a typical fluorescence lifetime of 2 ns, the expected fluorescence rejection ratio, in the absence of diffuse scattering, with a 4-ps gate is about 500:1 [Eq. (1)]. This rejection ratio is adequate for Raman spectroscopy, even under the highly unfavorable conditions of 400-nm excitation, where the remaining fluorescence background is approximately 10 to 12 times greater than the phosphate ν_1 (ca. 960 cm^{-1}) intensity. Underlying the spectra of Fig. 3 is an unrejected fluorescence background of approximately 2000 counts. For analysis and presentation purposes the background has been removed by subtraction of a baseline generated from a fitting to a third-order polynomial using 8 to 10 points in the spectrum where no Raman bands appear.

Table 1 Raman shift wavelengths and frequencies of bone tissue.

Wavelength (nm)	Raman shift (cm^{-1})	Literature value	Band assignment
415.9	958	959[a]	phosphate ν_1
417.9	1070	1070[a]	carbonate ν_1
421.2	1261	1255[a]	amide III
424.8	1460	1452[a]	CH_2 wag
428.1	1643	1640[b]	amide I
428.6	1669	1662[a]	amide I

[a] Bovine tissue, from Ref. 19.

[b] Human tissue, from B. R. McCreadie, M. D. Morris, T.-C. Chen, E. Widjaja, and S. A. Goldstein, unpublished observations.

The major bands in the Raman spectrum are identified in Fig. 3. All of the bands are attributable to bone mineral or bone matrix.[17] The replicate spectra provide an indication of the reproducibility of the measurement technique. In this case, uncertainty in the most intense bands is 2 cm^{-1} or less, and increases to 5 to 6 cm^{-1} for weaker bands. The 900-cm^{-1} spectral interval is sampled by 151 CCD pixels, corresponding to approximately 6 cm^{-1}/pixel. The sampling interval is adequate for the actual 15-cm^{-1} spectroscopic resolution. The peak frequency is reproducible to within 1 pixel, even for bands of low intensity, and can be estimated to within about 1/3 pixel for the strongest bands.

Table 1 compares the average band positions to those obtained with deep-red laser excitation and conventional instrumentation. In this table the wavelengths corresponding to the Raman shifts are also given. It should be noted that mineral bands can vary over a 2- to 3-cm^{-1} range, depending on the exact composition of the mineral. Typically the positions of bone matrix bands are less variable, but matrix (collagen) band intensities vary with the state of inter- and intra-fibril cross-linking in the specimen.

Bone tissue is only a moderately strong Raman scatterer and the spectra are noisier than those, for example, of transstilbene and polymers containing phenyl ring side chains obtained on the same instrument.[10] These molecules were the subject of the first full report of Raman photon migration and are known to generate intense Raman spectra. Additionally, because the 400-nm excitation scattered light passes into the Kerr gate, a Raman band from CS_2 at 795 cm^{-1} is generated that propagates through the optical train and is detected. Although the grating was positioned so that the detector collected Raman scatter down to 675 cm^{-1}, there are few features of interest below 850 cm^{-1} and the most characteristic bone bands occur in the 900- to 1700-cm^{-1} interval. To aid in reader assessment of the strengths and weaknesses of the technology and its prospects for further development, we have

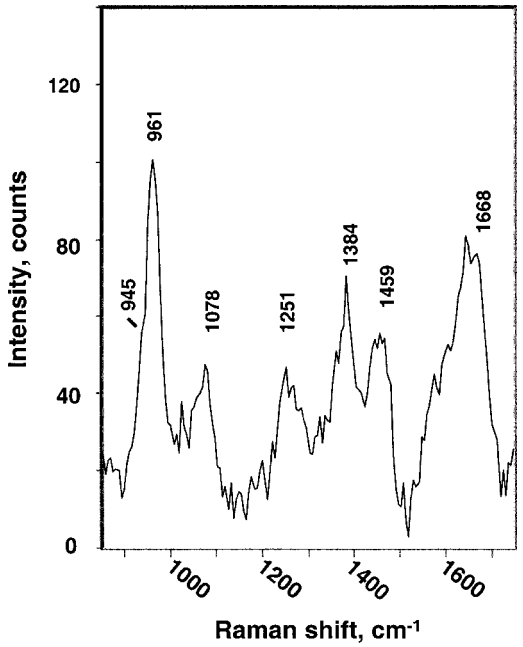

Fig. 4 Kerr-gated Raman spectrum of another specimen of equine cortical bone tissue. The measurement conditions are as in Fig. 3.

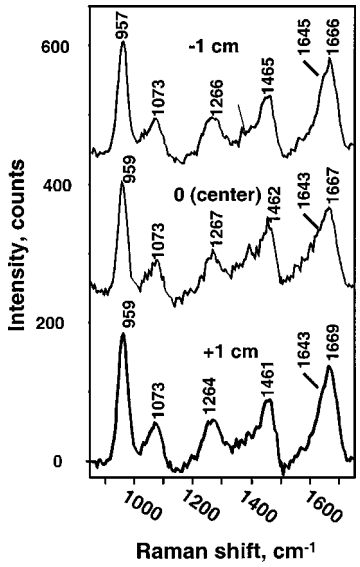

Fig. 5 Kerr-gated Raman spectra of another specimen of equine cortical bone tissue, showing point-point variations. The distances are along the long axis of the specimen. The measurement conditions are as in Fig. 3.

chosen to present raw data and not to hide any of these problems by using digital filtering, smoothing, or other methods for cosmetically improving the appearance of data. The spurious CS_2 signals can be eliminated by placing a blocking filter (e.g., holographic notch filter or an edge filter) in front of the Kerr gate preventing the 400-nm light from passing into the cell.

The detection of resonance Raman signals using the picosecond time-gating fluorescence rejection strategy represents a trade-off between spectral resolution and the level of fluorescence rejected. Our instrument is normally used for time-resolved resonance Raman spectroscopy, not Raman photon migration. Therefore it is configured for operation with a 1-ps, 1-kHz laser pulse train, which provides the best compromise between time and spectral resolutions in those experiments. As a consequence the instrument has a transform-limited spectral bandwidth of about 15 cm^{-1}. The result is that narrow Raman bands are broadened and some features of complex band envelopes are blurred or lost. For example, the phosphate ν_1 band (ca. 960 cm^{-1}) of bone tissue typically has a full width at half height of about 15 to 17 cm^{-1}. In these experiments using the short pulse duration time necessary for the gating this band is broadened to about 30 cm^{-1}. There are two consequences of this: first, the broadening of this peak means its intensity appears to be only slightly greater than the peak intensity of amide I. In Raman spectra obtained with instruments of 2- to 4-cm^{-1} resolution, the phosphate peak intensity is usually 3 to 4 times greater than the peak intensity of amide I in mature, fully mineralized tissue. Second, the shoulder normally observed at about 945 cm^{-1} is unresolved, as in Fig. 3. At best the shoulder is just visible, as in Fig. 4, which was obtained on another bone specimen. Even in this instance the shoulder is less prominent than in spectra obtained on an instrument that provides higher spectroscopic resolution. In Fig. 4 there is also a band at 1384 cm^{-1} that is observed because of the minimal specimen pretreatment employed in this study.

Similarly, some of the detail normally observed in the amide I envelope is lost because of the low resolution of the instrument. However, the amide I components are somewhat broader than the mineral bands and there may be less loss of information in the protein bands than in the mineral bands. We stress the problem is only one for our current instrument configuration. Most or all of the lost spectral detail could be recovered by using a pulse width of 3 ps (5 cm^{-1} resolution) and this would result in negligible deterioration of the Kerr gate 4-ps response time.

Further signs of spatial averaging are shown in Fig. 5, which shows Raman spectra obtained from the same specimen but at positions 1 cm apart along the long axis of the specimen. As in Fig. 3, the spectra are similar, suggesting that the average tissue composition is uniform on this spatial scale. However, the literature of both infrared and Raman microscopy of bone tissue contains many examples of local spatial variation within a 200-μm distance. Composition variation information is not available in these measurements because the 200-μm focus diameter of the laser beam averages detail that can be seen in maps or images with 1- to 10-μm lateral resolution, while the limited signal/noise ratio further obscures small local variations.

We next examined the effect of delaying the opening of the Kerr gate relative to the excitation pulse to monitor the temporal nature of the Raman signals and determine the depth of light penetration through a specimen of bone tissue. Figure 6 shows how the spectra varied with time under these conditions for a 0.22-mm-thick bone specimen placed in the optical path at 45 deg giving an effective depth of $\sqrt{2}\times 0.22 = 0.31$ mm. The spectrum of a piece of polystyrene placed behind the bone tissue serves as a marker of the arrival of Raman photons generated from depths greater than the tissue thickness.

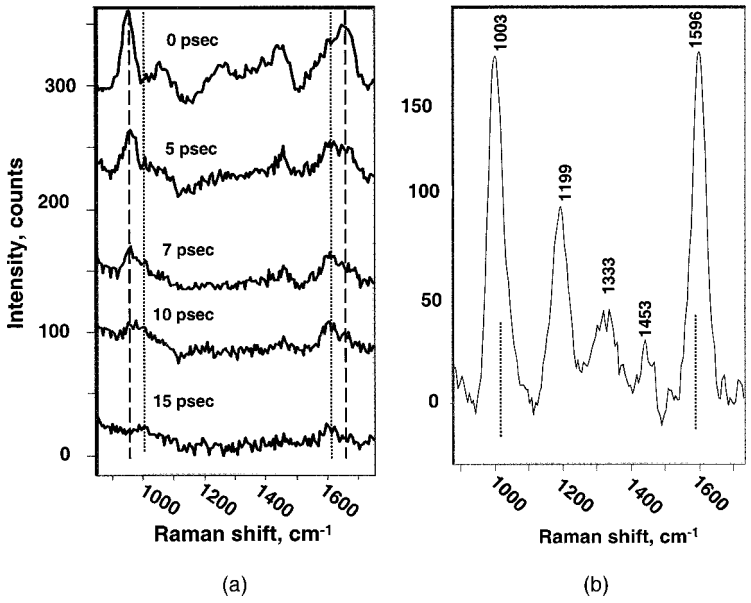

Fig. 6 Time-delayed Raman spectra of a specimen of equine cortical bone tissue. (a) The delay times are listed above each spectrum. The inverse square root of time decay of the intensity of the bone 960-cm^{-1} line (not shown) demonstrates that the signal arises primarily from diffusive photons. The dashed registration lines are centered on the bone 960-cm^{-1} and 1668-cm^{-1} bands. The dotted registration lines are centered on polystyrene 1001-cm^{-1} and 1604-cm^{-1} bands. (b) Polystyrene reference spectrum obtained with 0-ps gate delay time.

For comparison, a polystyrene spectrum obtained with zero gate delay is also shown.

The major bands of the polystyrene spectrum are discernable at a 15-ps delay. At a 20-ps delay both the bone tissue and polystyrene spectra were undetectable. Further confirmation of Raman photon diffusion is found by fitting the time dependence of the integrated area under the phosphate ν_1 band to a $t^{-1/2}$ decay.[11] Linear regression with $t^{-1/2}$ as the independent variable yields $r^2 = 0.998$.

Although there are no published refractive index measurements for bone tissue, the high mineral content means that the value should be similar to that of tooth enamel, i.e., about 1.6 in the visible spectral range. The transit time for a ballistic photon to reach the polystyrene through a 0.31-mm-thick medium of refractive index 1.6 is about 1.55 ps and the return time for a ballistic Raman photon is also about 1.55 ps. Therefore ballistic Raman scatter from polystyrene is expected at about 3.1 ps. Some polystyrene signal is seen at a 5-ps gate delay and this suggests that there is at least some ballistic component to the Raman spectrum. A purely diffusive polystyrene Raman component continues to appear in the time-delayed spectra until at least 15 ps.

The 0.31-mm path length used in these experiments may be close to the maximum obtainable with a 400-nm excitation wavelength. We attempted to make similar measurements with a 0.5-mm-thick specimen, also oriented at 45 deg to the laser propagation direction. In this case we were unable to observe any polystyrene signal.

Our experiments do allow us to estimate the amount of light lost by time-gating. In replicate experiments the zero delay time integrated intensity for the 960-cm^{-1} band was 43% to 52% of the integrated intensities for this band summed over the entire time-resolved sequence. Additional signal is generated between the sampling invervals. Conservatively, therefore, we can assume that time-gating with zero delay recovers no more than 40% of the available signal. The Kerr gate polarizers limit its transmission to 40%. The overall signal recovery at zero gate delay is about 40%×40%=16% of what would be available in a dc experiment, assuming no fluorescence problems.

4 Conclusions

The present study demonstrates that time-gated depth-resolved Raman measurements of tissue specimens are feasible. The measured spectra are similar to those obtained with more conventional spectrographic approaches, although broadened by the short pulse widths employed in this work. As in the more familiar absorbance and fluorescence cases, in Raman spectroscopy a diffusive process may blur depth information. In principle it should be able to recover subsurface Raman spectroscopic detail of highly scattering tissues using the techniques developed for photon migration in absorbance and fluorescence measurements.

Of particular note is that even with deep-blue laser excitation and our unoptimized instrumentation, depth penetration through bone tissue of about 0.3 mm is shown to be feasible. There are no instrumentation limitations that require the use of 400-nm excitation. An upgraded version of our instrument will be configured to use 800-nm Raman excitation. At this wavelength the depth of penetration would increase to 1 mm or more. This approach is presently being tested and will be the main focus of future studies. Experiments with this instrument will be reported at a later date.

Ultimately, these preliminary results demonstrate that Raman photon migration is feasible in tissue, with a depth of penetration commensurate with other spectroscopies at similar wavelengths. Photon migration may also provide a simple and effective means to improve discrimination between Raman scatter from bone matrix and from the spectroscopically simi-

lar collagen of skin tissue. There is every reason to believe that noninvasive transcutaneous measurements of bone tissue to depths of at least 1 to 2 mm are possible with the present instrumentation used here.

Some consideration needs to be made when using near-infrared excitation because, in the absence of fluorescence, longer gating times may be more appropriate. For example a streak camera may be a viable instrument for diffuse Raman measurements for the collection of deep zone Raman photons that are delayed over 100 ps or even several hundred picoseconds. A wider gate width of tens or hundreds of picoseconds may also be beneficial. Conventional gated intensified cameras or even Pockels cells functioning as gates may also be adequate. Any of these slower time-resolved systems would be less expensive to implement than our current apparatus optimized for ultrafast TR^3 studies. In such situations, however, fluorescence rejection capability might be compromised and so further work is necessary to establish the optimum conditions.

The potential for *in vivo* monitoring of bone disease using the molecular specific capabilities of Raman spectroscopy are very exciting. While the potential utility for human subjects is clear, *in vivo* capability would also be advantageous in small animal studies. In those applications it could reduce or eliminate the need for sacrificing a large number of animals to study tissue properties over all or part of the life cycle. It may also be possible to distinguish between cortical and trabecular bones in small animals, further increasing the range of noninvasive *in vivo* studies.

Acknowledgments

M.D.M. acknowledges financial support through NIH grant R01 AR47969 and the University of Michigan Core Center for Musculo-Skeletal Research (NIH grant P30 AR46024) and travel support from the Rackham Graduate School, University of Michigan. We thank CCLRC for granting access to the Central Laser Facility to perform this work.

References

1. T. Vo-Dinh, *Biomedical Photonics Handbook*, CRC Press, Boca Raton, FL (2003).
2. A. Mahadevan-Jansen and R. Richards-Kortum, ''Raman spectroscopy for the detection of cancers and precancers,'' *J. Biomed. Opt.* **1**, 31–70 (1996).
3. T. C. Bakker Schut, M. J. H. Witjes, H. J. C. M. Sternborg, O. C. Speelman, J. L. N. Roodenburg, E. T. Marple, H. A. Bruining, and G. J. Puppels, ''In vivo detection of dysplastic tissue by Raman spectroscopy,'' *Anal. Chem.* **72**, 6010–6018 (2000).
4. N. Stone, C. Kendall, N. Shepherd, P. Crow, and H. Barr, ''Near-infrared Raman spectroscopy for the classification of epithelial precancers and cancers,'' *J. Raman Spectrosc.* **33**, 564–573 (2002).
5. A. Mahadevan-Jansen, ''Raman spectroscopy: from benchtop to bedside,'' in *Biomedical Photonics Handbook*, T. VoDinh, Ed., pp. 30-1–30-27, CRC Press, Boca Raton, FL (2003).
6. J. J. Baraga, M. S. Feld, and R. P. Rava, ''In situ optical histochemistry of human artery using near infrared Fourier transform Raman spectroscopy,'' *Proc. Natl. Acad. Sci. U.S.A.* **89**, 3473–3477 (1992).
7. P. J. Caspers, G. W. Lucassen, H. A. Bruining, and G. A. Puppels, ''Automated depth-scanning confocal Raman microspectrometer for rapid in vivo determination of water concentration profiles in human skin,'' *J. Raman Spectrosc.* **31**, 813–818 (2000).
8. J. Wu, Y. Wang, L. Perelman, I. Itzkan, R. Dasari, and M. S. Feld, ''Three-dimensional imaging of objects embedded in turbid media with fluorescence and Raman spectroscopy,'' *Appl. Opt.* **34**, 3425–3430 (1995).
9. C. J. H. Brenan and I. W. Hunter, ''Volumetric Raman microscopy through a turbid medium,'' *J. Raman Spectrosc.* **27**, 561–570 (1996).
10. N. Everall, T. Hahn, P. Matousek, A. W. Parker, and M. Towrie, ''Picosecond time-resolved Raman spectroscopy of solids: capabilities and limitations for fluorescence rejection,'' *Appl. Spectrosc.* **55**, 1701–1708 (2001).
11. N. Everall, T. Hahn, P. Matousek, A. W. Parker, and M. Towrie, ''Photon migration in Raman spectroscopy,'' *Appl. Spectrosc.* **58**, 591–597 (2004).
12. P. P. Yaney, ''Reduction of fluorescence background in Raman spectra by the pulsed Raman technique,'' *J. Opt. Soc. Am.* **62**, 1297–1303 (1972).
13. J. Lakowicz, *Principles of Fluorescence Spectroscopy*, 2nd ed., pp. 64–66, Kluwer Academic/Plenum Publishers, New York (1999).
14. P. Matousek, M. Towrie, A. Stanley, and A. W. Parker, ''Efficient rejection of fluorescence from Raman spectra using picosecond Kerr gating,'' *Appl. Spectrosc.* **53**(12), 1485–1489 (1999).
15. P. Matousek, M. Towrie, and A. W. Parker, ''Fluorescence background suppression in Raman spectroscopy using combined Kerr gated and shifted excitation Raman difference techniques,'' *J. Raman Spectrosc.* **33**, 238–242 (2002).
16. H. Hamaguchi and T. Tahara, ''Picosecond Raman spectroscopy using a streak camera,'' *Appl. Spectrosc.* **47**, 391–398 (1993).
17. A. Carden and M. D. Morris, ''Application of vibrational spectroscopy to the study of mineralized tissues,'' *J. Biomed. Opt.* **5**(3), 259–268 (2000).
18. C. P. Tarnowski, M. A. Ignelzi, Jr., and M. D. Morris, ''Mineralization of developing mouse calvaria as revealed by Raman microspectroscopy,'' *J. Bone Miner. Res.* **17**(6), 1118–1126 (2002).
19. A. Carden, R. M. Rajachar, D. H. Kohn, and M. D. Morris, ''Ultrastructural changes accompanying the mechanical deformation of bone tissue: a Raman imaging study,'' *Calcif. Tissue Int.* **72**(3), 166–175 (2003).
20. P. Matousek, M. Towrie, C. Ma, W. M. Kwok, D. Phillips, W. T. Toner, and A. W. Parker, ''Fluorescence suppression in resonance Raman spectroscopy using a high performance picosecond Kerr gate,'' *J. Raman Spectrosc.* **32**, 983–988 (2001).